# Islanding Detection for Active Distribution Networks Using a WaveNet+UNet Classifier

Amirhosein Alizadeh, Seyed Fariborz Zarei, and Mohammadhadi Shateri

***Abstract*—This paper proposes an AI-based approach for islanding detection in active distribution networks. A review of existing AI-based studies reveals several gaps, including model complexity and stability concerns, limited accuracy in noisy conditions, and limited applicability to systems with different types of resources. To address these challenges, this paper proposes a novel approach that adapts the WaveNet generator into a classifier, enhanced with a denoising UNet model, to improve performance in varying signal-to-noise ratio (SNR) conditions. In designing this model, we deviate from state-of-the-art approaches that primarily rely on long short-term memory (LSTM) architectures by employing 1D convolutional layers. This enables the model to focus on spatial analysis of the input signal, making it particularly well-suited for processing long input sequences. Additionally, residual connections are incorporated to mitigate overfitting and significantly enhance the model's generalizability. To verify the effectiveness of the proposed scheme, over 14 000 islanding/non-islanding cases are tested, considering different load active/reactive power values, load switching transients, capacitor bank switching, fault conditions in the main grid, different load quality factors, SNR levels, changes in network topology, and both types of conventional and inverter-based sources.**

***Index Terms*—Active distribution networks, distributed generation, inverter-based resources, islanding detection, UNet denoising model, WaveNet model.**

## I. Introduction

Islanding is a condition where portions of the power network become electrically isolated from the main grid while continuing to generate and consume electricity autonomously [1]. This presents a significant challenge for distribution system operators when dealing with active distribution networks [2]. From an electrical perspective, islanding can lead to voltage and frequency fluctuations, degraded power quality, and potential damage to infrastructure components [3]. From a safety perspective, islanding poses a considerable risk to line workers who may be unaware of localized energized islands during maintenance tasks [4]. Thus, it is essential to detect islanding conditions to ensure the reliability of the system and protect personnel [5]. Islanding detection methods encompass diverse categories in terms of principles and techniques, including classical, remote, and modern schemes [6]. All methods should adhere to a detection time of up to 2.0 seconds based on IEEE 1547-2018 [7]. Within classical methods, both passive and active techniques exist. In the passive method, variations in system parameters are monitored based on measured signals [8], whereas the active method injects power signal perturbations into the power grid to increase sensitivity [9]. Examples of classical methods include the adaptive rate of change of frequency (ROCOF) islanding detection relay [10], THD-based detection [11], impedance measurement-based detection [12], injection approach based on the maximum power point tracking concept for islanding detection in photovoltaic systems [13], feasibility study of intentional islanding of conventional sources [14], statistical feature for islanding detection in the presence of inverters [15], and space vector domain islanding detection [16]. In the second category, the remote schemes rely on information exchange while their processing technique is similar to classical methods [17]. In the third category, modern methods analyze electrical signals using signal processing tools to identify islanding conditions [18], such as real-time wavelet analysis [19] and artificial intelligence (AI)-based approaches, which use historical data to learn the islanding patterns [20].

Recent work has emphasized the superiority of the AI-based approaches [21], [22]. These methods can learn complex nonlinear patterns and eliminate the need for threshold adjustments required by other techniques [23]. In [24], a technique using support vector machines (SVM) is proposed for inverter-based distributed generation with 60 input features. Additionally, reference [25] employs a K-nearest neighbors (KNN) methodol-

Received: December 21, 2024
Accepted: March 31, 2025
Published Online: September 1, 2025
Amirhosein Alizadeh and Seyed Fariborz Zarei (corresponding author) are with the Department of Electrical and Computer Engineering, Qom University of Technology, Qom 3718146645, Iran (e-mail: alizadeh.ah@gmail.com; zarei@qut.ac.ir).
Mohammadhadi Shateri is with the Systems Engineering Department, Ecole de technologie superieure, Montreal H3C 1K3, Canada (e-mail: mohammadhadi.shateri@ etsmtl.ca).
DOI: 10.23919/PCMP.2024.000404

ogy for islanding detection in grid-tied solar PV systems. Such schemes have achieved an accuracy of up to 97%. In recent years, recurrent neural networks (RNN) based on long short-term memory (LSTM) have been proposed [26], achieving accuracy values exceeding 99%. Specifically, reference [27] proposes a microgrid islanding detection method using a multi-feature LSTM network, while [28] includes an inverter-based source and in [29], a scheme based on harmonic signals within a multi-LSTM structure is used for islanding detection. More sophisticated approaches, such as those in [29], combine convolutional neural networks (CNNs) and LSTM architectures to detect islanding in a system with both inverter-based and synchronous-based sources. Despite achieving islanding detection accuracy of over 99%, these models suffer from high computational complexity and instability in noisy conditions [4], [30].

To further investigate the performance of islanding detection methods, particularly in noisy conditions, the LSTM-based methods in [27] and [31] achieve an islanding detection accuracy of 97% in SNR conditions of 30 dB. In [32], tests conducted on an IEEE13-bus network with four resources result in a near-zero NDZ. However, although noise conditions are examined up to 30 dB, the study does not provide accuracy metrics for the proposed method. In contrast, reference [33] reports an accuracy of 99.9% using the cubature kalman filtering algorithm (CKFA) on an IEEE13-bus system with two resources, but its performance in noisy conditions is not evaluated. Similarly, reference [34] claims an accuracy of 99.9%, no noise immunity is discussed in its tests. The accuracies of methods in [35]–[37] decrease to 98%, 96.13%, and 96.66%, respectively, in noisy conditions. In references [38] and [39], tests with noise levels up to 30 dB result in accuracies of 98% and 97.09%, respectively.

To address these shortcomings, this study introduces a novel method based on the WaveNet model for islanding detection [40]. WaveNet was originally designed by Google DeepMind for autoregressive audio generation through modeling the temporal dependencies within audio data. The backbone of the proposed model is an adapted WaveNet architecture, where the original generator is transformed into a classifier by adding a classifier head (i.e., a fully connected layer with a sigmoid activation function). This modification enables the prediction of the likelihood of islanding occurrence. In designing this model, 1D convolutional layers are employed, allowing it to analyze the input signal spatially rather than relying on sequential dependencies. This design choice avoids difficulties related to the modelling of long-term dependency often associated with LSTM architectures, making the model more efficient for analyzing long input sequences. Additionally, residual (or skip) connections are incorporated which mitigate the vanishing gradient problem and significantly enhance the model's generalization capacity. To ensure high detection accuracy even under severe noise, a novel feature denoising step is introduced by integrating a UNet model, which acts as an adaptor for the WaveNet model, enabling reliable performance across a broad range of signal-to-noise ratio (SNR). The comparative analysis demonstrates that the proposed single WaveNet model exhibits greater robustness to noise, with a complexity reduced by more than half compared to existing state-of-the-art islanding detection models. Furthermore, integrating WaveNet with UNet denoising significantly enhances islanding detection accuracy, achieving up to 98% accuracy even in substantial noise levels with a 10 dB SNR. The effectiveness of the proposed approach is rigorously assessed through comprehensive testing across diverse real-world scenarios, including both islanding and non-islanding conditions. Moreover, the validation process employs a realistic test system incorporating both conventional and inverter-based resources. The key contributions of this study are as follows.

1) A novel islanding detection model is introduced based on the WaveNet framework, wherein the generative architecture is adapted into a classifier to predict the likelihood of islanding occurrence. By using 1D convolutional layers and incorporating residual connections, the model spatially analyzes input signals, effectively addressing the limitations of modelling the long sequential dependency in LSTM-based approaches. The findings demonstrate that this adaptation achieves better performance than state-of-the-art methods, while reducing computational complexity by more than half. To the best of our knowledge, this work represents the first adaptation of WaveNet for islanding classification.

2) To enhance the robustness of WaveNet-based islanding detection in noisy environments, a feature denoising mechanism is proposed by integrating a pre-trained UNet model. Unlike the conventional pre-processing step, the UNet dynamically acts as an adaptor for our WaveNet islanding detector during inference, performing denoising without prior knowledge of noise severity. This integration significantly improves the model's performance in severe noise conditions, ensuring reliable operation across a wide range of SNRs.

3) The performance of the proposed WaveNet-based islanding detection, both stand-alone and integrated with UNet feature denoising, is thoroughly evaluated against state-of-the-art methods across diverse islanding and non-islanding scenarios at different SNRs. The proposed WaveNet model, when augmented with the denoising UNet, demonstrates a significant performance enhancement, achieving an accuracy greater than 98% at 10 dB SNR.

The subsequent sections of this paper are structured as follows. Section II presents the test system and details

the islanding simulation process, while Section III outlines the deep learning-based islanding detection classifiers, introducing the proposed WaveNet classifier alongside the UNet denoising step designed to enhance detection accuracy. Section IV details the experimental findings, providing a comparative analysis with the LSTM-based islanding classifier in terms of computational complexity and accuracy across varying noise levels. Finally, Section V concludes the study by summarizing the key findings and contributions.

This paper uses uppercase letters to denote random variables and lowercase letters to signify specific realizations or values. The notation $P(x)$ represents the probability distribution of the random variable $X$, while $E[\cdot]$ denotes the expectation operator with respect to the joint distribution of all pertinent random variables. Additionally, $E[Y|X]$ denotes the conditional expectation of $Y$ given $X$. For a sequence of random variables, or a time series, of length $T$, denoted by $X^T = (X_1, X_2, \cdots, X_T)$, the corresponding realization is represented by $x^T = (x_1, x_2, \cdots, x_T)$. The sigmoid function is defined as $\sigma(z) = \dfrac{1}{1+\mathrm{e}^{-z}}$ and the hyperbolic tangent function is given by $\tanh(z) = \dfrac{1-\mathrm{e}^{-2z}}{1+\mathrm{e}^{-2z}}$.

## II. Test System and Islanding Simulation

The system under study is based on the IEEE33-bus test system, as illustrated in Fig. 1. This system comprises the utility distribution network, referred to as the Grid, connected at node 1. It also includes a 250 kW grid-connected photovoltaic plant, denoted as the PV unit, connected at node 33, a 2 MW synchronous generator identified as DG, connected at node 18, and a 1.5 MW doubly-fed induction generator (DFIG) wind turbine, referred to as Wind, connected at node 25. All components are illustrated in Fig. 1, with their corresponding parameters listed in Table I.

The solar PV plant analyzed in this study has a capacity of 250 kW, with its technical specifications detailed in Table I. The system comprises 86 parallel strings, each consisting of seven SunPower SPR-415E modules connected in series. This configuration is linked to an inverter using a three-level IGBT-based design. The PV inverter is connected to a step-up transformer (250 kVA, 3-phase, 250 V/25 kV, T3). Power is transmitted through a 4 km distribution line to a step-down transformer (250 kVA, 25 kV/400 V, 3-phase, T2) and the 400 V side of this transformer is then connected to node 33 of the distribution system [41]. Additionally, a synchronous generator with a capacity of 3 MVA operates at 400 V, 50 Hz, and 1500 rpm. Driven by a diesel engine, this generator is linked to node 18, located 500 meters from the system. A 1.5 MW variable speed DFIG wind turbine (575 V, 50 Hz) is integrated with the grid through a 1750 kVA, 3-phase, 400 V/575 V transformer (T4) located at node 25 [42].

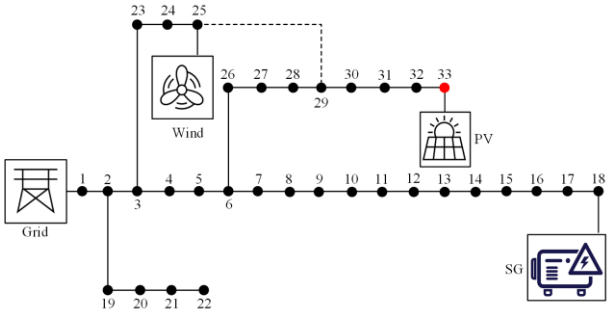


Fig. 1. Schematic of the modified IEEE33-bus standard test system with grid-connected photovoltaic plant, synchronous generator, and DFIG wind turbine.

TABLE I
Parameters of the Test System

| Parameters | Values |
|---|---|
| PV arrays | 86 times 7 modules |
| PV modules | SunPower SPR-415E |
| DG system | 3 MVA, 400 V, 50 Hz, 1500 rpm |
| Wind turbine | 1.5 MVA, 575 V, 50 Hz |
| T1 | 25 kV/400 V; 10 MVA |
| T2 | 25 kV/400 V; 250 kVA |
| T3 | 250 V/25 kV; 250 kVA |
| T4 | 575 V/400 V; 1750 kVA |
| R1 and L1 for all lines | 1.273 mΩ/km; 0.9337 mH/km |
| R0 and L0 for all lines | 38.64 mΩ/km; 4.1264 mH/km |
| Load 1 | 1.2 MW; 0.3 MVAR; at node 22 |
| Load 2 | 0.6 MW; 0.2 MVAR; at node 29 |

Data gathering is the fundamental step in implementing islanding detection methods. Generally, samples of electrical quantities at the point of connection between distributed generation and the distribution system are measured and used. In this paper, the measured quantities at the point where the PV source is connected to node 33 are considered. The measured data include current and voltage waveforms sampled at a frequency of 1 kHz. These sampled data are employed to extract various electrical quantities that serve as additional features for detection processes. In this study, a set of five electrical features is used, including positive, negative, and zero sequence voltages, ROCOF, and the superimposed voltage waveforms. To explain the feature selection process, a literature review reveals that there are approximately 63 available features encompassing parameters associated with voltage, current, power, and their combinations. Because of the increased computational demands and hindered detection speed associated with using such a large number of features, using all of them is not feasible, and it is necessary to reduce the number of features and only select the most effective ones.

In this paper, the selection is narrowed down to the five best features from an initial pool of 63, using filter-based strategies and wrapper-based feature selection techniques [43]. The aim is to derive the resulting features by combining subsets of the possible 63. Initially, the 63 features are divided into groups of five to assess the effect of each group. Four groups that yield the best results are then identified, while the impact of each remaining feature is evaluated individually. Subsequently, ten that produce the best outcomes are selected. Finally, various combinations of five features from the set of ten are assessed to identify the combination that provides the best possible results as the final features. These are then considered inputs for the proposed UNet+WaveNet scheme. As a result, a combination of five features, including positive, negative, and zero sequence voltages, ROCOF, and superimposed voltage waveforms, demonstrates superior performance among all combinations and is chosen as the final set. This reduction in the number of used features significantly decreases computational burden. Figure 2 illustrates the schematic diagram of the proposed approach, where the measured three-phase voltage waveforms undergo processing through the feature extraction block to identify the necessary features for the UNet+WaveNet scheme. In Fig. 2, section (1) represents three-phase voltages measurement. Section (2) is feature extraction block. Section (3) is Unet + WaveNet classifier. Section (4) is islanding status signal output.

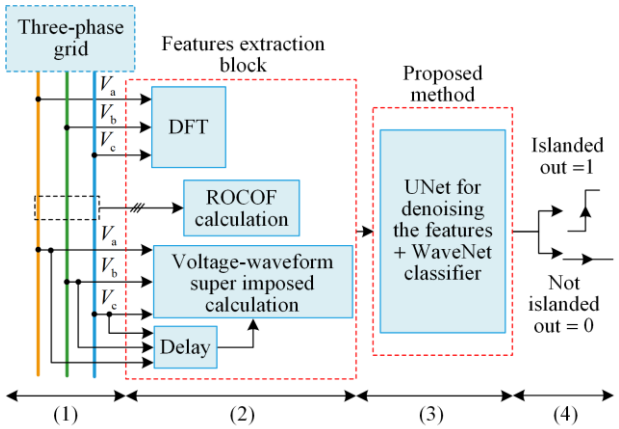


Fig. 2. Block diagram of the proposed algorithm for the islanding detection method.

Different scenarios for islanding and non-islanding states are assessed to evaluate various conditions and test the performance of the proposed method. In islanding conditions, the evaluation involves opening CB1 (the circuit breaker on the grid side) at node 2, intended to isolate the test network from the primary electrical grid. This test is conducted across 50 different active power levels and 30 diverse reactive power settings, resulting in a total of 1500 load configurations examined at various points in the network. Additionally, different quality factors ranging from 1 to 2.5 (in accordance with international standards) and various network points with differing distances between resources are used, all yielding similar results. To further evaluate the effectiveness of the proposed method within the zero-power mismatch range, 605 distinct points of active power ($P$) and reactive power ($Q$) are analyzed. This assessment is conducted with an accuracy of 0.05% (within ±0.008 p.u. for ΔP and ±0.03 p.u. for $\Delta Q$), and a precision of 0.001 p.u. for ΔP and 0.002 p.u. for $\Delta Q$, ensuring maximum precision in evaluating the proposed method. Also, the system performance is specifically tested at $\Delta P = 0$ and $\Delta Q = 0$.

In non-islanding scenarios, various conditions are tested, including: 1) the entry and exit of different loads with varying qualities at different times and locations within the network; 2) connecting and disconnecting capacitor banks at various grid locations at different timings and values; 3) applying different short-circuit faults, including LG, LL, LLG, and LLL faults at different locations with varying resistances; 4) disconnection and reconnection of resources in adjacent feeders; 5) changes in network topology by establishing a connection between nodes 25 and 29; and 6) considering various noise levels ranging from 40 dB to 5 dB across seven distinct levels.

A total of 14 266 time-series data samples are generated, including 5132 islanded samples, with the remainder categorized as non-islanded. Details regarding data analysis and islanding detection will be discussed in Section IV.

## III. Proposed Deep Classifiers for Islanding Detection

In this section, the classification approach based on deep neural networks for islanding detection is introduced. This network receives a time series as input which consists of features extracted from the voltage and current of an active distribution network and returns the likelihood of islanding occurrence at the output. More precisely, consider the time-series $X^T$ where for each $t \in \{1, 2, \cdots, T\}$, $X_t$ takes values on $R^d$, where $d$ refers to the number of features considered at time $t$. The random variable $Y$ is defined as the islanding label associated with each $X^T$, where $Y \in Y = \{0, 1\}$ and 1 refers to islanding. Thus, while $p(y \mid x^T)$ is the true probability distribution of the islanding labels given the time-series features $x^T$, the goal of the deep neural network classifier is to predict $q(y \mid x^T)$ as an approximation of the true distribution $p(y \mid x^T)$ through minimizing the Kullback-Leibler (KL) divergence [44]:

$$\inf_{q_{Y|X^T}} \mathrm{KL}(p_{YX^T} \,\|\, q_{YX^T}) = \inf_{q_{Y|X^T}} E\left[\log \frac{p_{Y|X^T}(Y \mid X^T)}{q_{Y|X^T}(Y \mid X^T)}\right] \quad (1)$$

where the expectation is taken concerning the true distribution $p_{YX}^{T}$. Solving the optimization problem (1) is equivalent to minimizing $E\left[-\log q_{Y|X^T}(Y \mid X^T)\right]$, known as the cross-entropy. Throughout this study, the cross-entropy serves as the loss function, employed as the objective function.

### *A. LSTM Classifier*

RNNs constitute a class of neural networks explicitly tailored for sequential data. Each RNN unit processes an input along with its hidden state from the previous time step thus enabling the capture of the dynamics of sequential data over time. Figure 3(a) represents the principles of RNNs, where both networks $f$ and $g$ are modeled by fully connected (FC) layers. While RNNs are adept at capturing short-term dependencies, they struggle to retain information over longer sequences because of vanishing gradients [45]. This limits their practicality in scenarios requiring an understanding of context beyond recent history. LSTM networks, introduced in [46] and subsequently refined in [47], enrich RNNs by integrating specialized memory cells and gating mechanisms. LSTMs are equipped with the capability to selectively store and retrieve information across extended sequences. (see Fig. 3(b)).

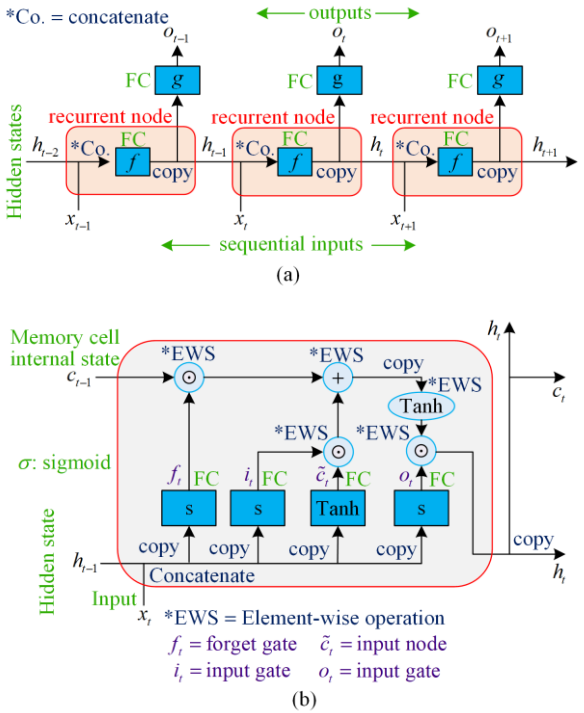


Fig. 3. Recurrent architectures used in this work. (a) Vanilla RNN unrolled over time. (b) LSTM cell showing input, forget, and output gates.

There are three key components that enable long-term modeling in LSTM including: 1) the forget gate that controls the memory's internal state and determines whether to keep it (important information) or flush it (remove the irrelevant information); 2) the output gate that determines the impact of the cell on the output at the current time; and 3) the input gate and input node that determine how much information from the input should be added to the memory. At the end, the output of the cell, i.e., the hidden state (which will be applied to the next time step) is generated. The equations representing the formulations of LSTM nodes at time step $t$ are as follows:

$$\begin{aligned} f_t &= \sigma(b^f + K^f h_{t-1} + V^f x_t) \\ i_t &= \sigma(b^g + K^i h_{t-1} + V^i x_t) \\ \tilde{c}_t &= \sigma(b^{\tilde{c}} + K^{\tilde{c}} h_{t-1} + V^{\tilde{c}} x_t) \\ o_t &= \sigma(b^o + K^o h_{t-1} + V^o x_t) \\ c_t &= f_t \times c_{t-1} + i_t \times i_t \\ h_t &= o_t \times \tanh(c_t) \end{aligned} \tag{2}$$

where $b$, $K$, and $V$ represent biases, input weights, and recurrent weights associated with each gate, respectively. Stacking multiple LSTM layers and culminating in a fully connected layer with sigmoid activation significantly enhances the classification of the input time series.

### *B. WaveNet Classifier*

WaveNet is a generative model designed by DeepMind for synthesizing raw audio waveforms [40]. Unlike traditional methods that generate audio by modeling spectrograms or other high-level features, WaveNet operates directly on the raw waveform data by autoregressive modeling of the audio probability distribution. More precisely, consider the sequence of random variables $X^T = (X_1, X_2, \cdots, X_T)$ of length $T$ where for each $t \in \{1, 2, \cdots, T\}$, $X_t$ takes values on $R^d$. Using the chain rule of probability, $p(x^T)$, as the probability distribution of sequential data $X^T$, can be written as follows:

$$p(x^T) = p(x_1)p(x_2 \mid x_1)\cdots p(x_T \mid x_{1:T-1}) = \prod_{t=1}^{T} p(x_t \mid x_{1:t-1}) \tag{3}$$

where $p(x_1 \mid x_{1:0}) \coloneqq p(x_1)$. Equation (3) is called the autoregressive modeling of $p(x^T)$, and WaveNet aims to learn $p(x^T)$ through modeling each of the conditional probability terms. To this end, WaveNet employs a dilated causal convolutional architecture, inspired by the idea of dilated convolutions that effectively increase the receptive field (the number of previous times that impact the output at time $t$) without a corresponding increase in parameters. To understand the concept of dilated convolutions, considering a filter sliding over the input data, it jumps with increasing gaps instead of

only moving one step at a time. This is called a dilated convolution. These gaps, or dilation rates, determine how much context the model considers while making predictions. In addition, to ensure the causality observed in (3), WaveNet only uses information from the past to predict the future. Thus, the core of WaveNet is its stack of dilated causal convolutional layers (see Fig. 4).

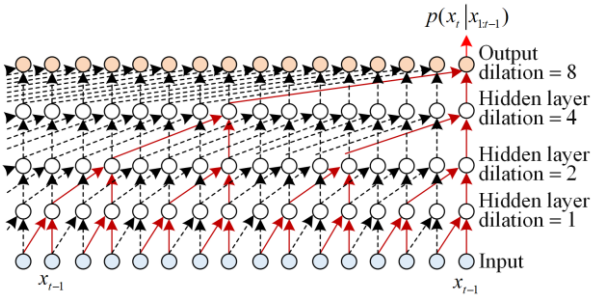


Fig. 4. An example of a stack of causal convolutional layers inspired by [40].

The bold red arrows highlight the connections linking the output at time $t$ with previous layers. This structure allows for capturing the conditional term $p(x_t \mid x_{1:t-1})$ based on the latest 16 input time steps, which corresponds to a receptive field of size 16.

To improve the strength of the WaveNet model, gated activation units, an idea inspired by the LSTM gating mechanism, is incorporated into designing WaveNet [40]. More precisely, each convolutional layer is composed of a gated activation unit which consists of two parallel branches-one for the filter and another for the gate. Assuming $x^T$ and $z^T$ as the input and output of the $k$th layer in the WaveNet network, the gated activation is modeled as follows:

$$z^T = \tanh(W_{f,k} \cdot x^T) \odot \sigma(W_{g,k} \cdot x^T) \qquad (4)$$

where $W_{f,k}$ and $W_{g,k}$ are the filter and gate parameters of the $k$th layer; and $\odot$is the element-wise product or Hadamard product. The filter-branch learns to extract relevant features from the input, while the gate branch controls the information flow. This helps prevent vanishing gradients and allows the WaveNet model to capture complex dependencies.

On top of this gated activation, to facilitate the learning of residual representations while simultaneously enhancing the ability to capture fine-grained features, skip connections, also known as residual connections, are used [48]. This simple idea enables the direct transfer of information from input to output and thus speeds up the convergence while enabling the training of a deeper WaveNet model (see Fig. 5(a)).

So far, WaveNet for generating time-series samples (e.g. audio) has been presented. To enable classification, the output of the WaveNet model is connected to a fully connected layer with one output and a Sigmoid activation function. The whole model is presented in Fig. 5(b). In this model, the FC refers to a fully connected layer.

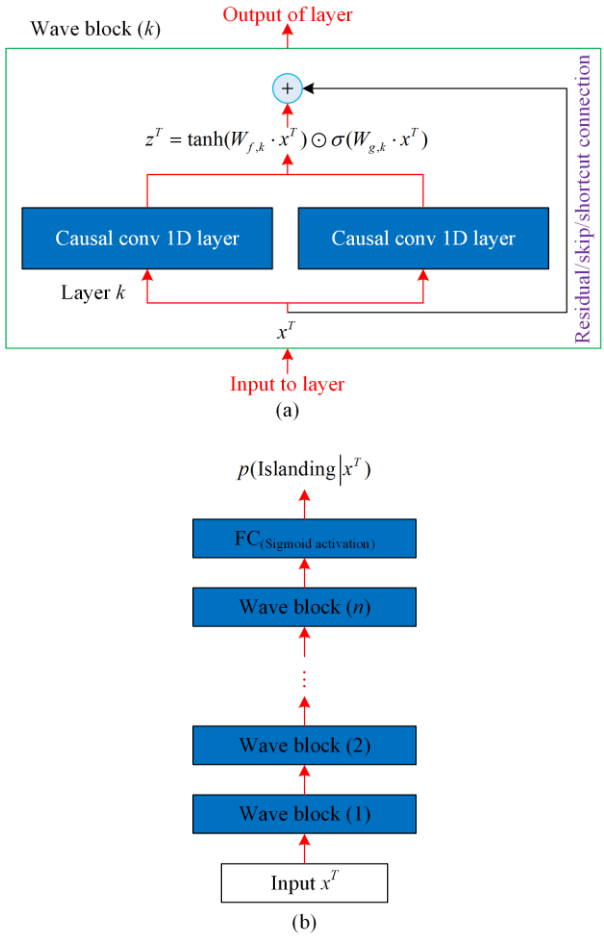


Fig. 5. WaveNet-based classifier for islanding detection. (a) Gated activation unit with residual/skip connections inside a WaveNet block. (b) Full WaveNet classifier with FC+sigmoid head producing islanding probability.

### *C. Feature Denoising with UNet Model*

The UNet architecture, initially proposed in [49] for biomedical image segmentation, has been adapted for various image processing tasks, including signal denoising. This paper presents an adaptation of the UNet model tailored for 1D signal denoising using CNNs. Comprising a contracting path (or encoder) followed by an expansive path (or decoder), the UNet architecture efficiently captures context and reduces spatial dimensions through the contracting path, while enabling precise localization via the expansive path (see Fig. 6).

The numbers at the output of each layer represent the size of the feature map. Note that in our pre-trained UNet model, the length of the input features is reduced by a factor of two at each UNet level in the encoding path and then it is increased by a factor of two at each level of the decoding path.

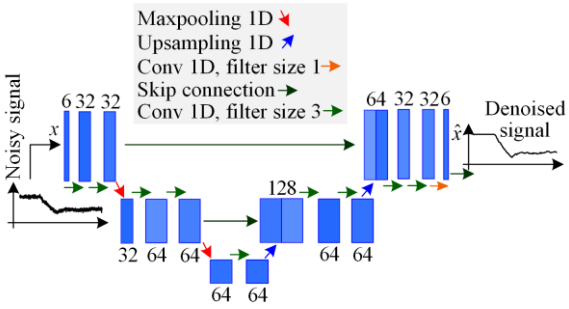


Fig. 6. UNet framework for denoising islanding features.

The contracting path comprises multiple layers of convolutional and max-pooling operations. Here, $x$ denotes the input signal, and $C_k$ represents the $k$th convolutional layer with a kernel size of 3, and a rectified linear unit (ReLU) activation function denoted by $\sigma$:

$$C_k(x) = \sigma(W_k \cdot x + b_k) \tag{5}$$

where $W_k$ and $b_k$ are the learnable weights and biases of the $k$th convolutional layer, respectively. The max-pooling operation reduces the spatial dimensions of the feature maps.

The expansive path consists of up-sampling followed by convolutional operations. Let $U_k$ represent the $k$th up-sampling layer, and $D_k$ denote the $k$th convolutional layers. These are followed by up-sampling layers, which increase the spatial resolution of the feature maps.

$$\begin{aligned} U_k(x) &= \text{Upsampling}(x) \\ D_k(x) &= \sigma(W_k' \cdot x + b_k') \end{aligned} \tag{6}$$

where $W_k'$ and $b_k'$ are the learnable weights and biases of the $k$th convolutional layer in the expansive path, respectively. The UNet model is trained by minimizing a reconstruction loss function, typically the mean absolute error or mean squared error, between the output and the clean (non-noisy) signal.

## IV. Results and Discussion

### A. Data Simulation and Models Structures

This study uses a dataset comprising 14 266 time-series data samples, each spanning a duration of 10 ms and including five features, as detailed in Section II. The dataset is divided into training and test sets with an 80–20 split. During the training phase, 20% of the training data is set aside as validation data to fine-tune hyper-parameters such as learning rate, number of layers, and the number of nodes in each layer. Details of the models' structures are provided in Table II. To ensure consistency and enhance model performance, the data is standardized using statistical parameters derived from the training dataset. Specifically, the mean and standard deviation of each feature are calculated based solely on the training data. These parameters are then used to transform the training, validation, and test datasets. Ensuring that all features have zero mean and unit variance guarantees the model's input features are appropriately normalized.

TABLE II
Comprehensive Comparison of the Performance of Various Models Based on Evaluation Metrics Applied to Test Data Samples

| Model | Model complexity | F1-score | Balanced accuracy | Precision | Recall |
|---|---|---|---|---|---|
| WaveNet classifier (ours) | Total of five wave blocks where each has 3 convolutional layers with filter size 32 (training parameters: 89 505) Adam optimizer with learning rate 0.0002 | 0.9988 ± 0.0003 | 0.9974 ± 0.0009 | 0.9977 ± 0.0008 | 0.9998 ± 0.0010 |
| LSTM classifier (state-of-the-art, [27], [28]) | 4 LSTM layers with 64, 128 64, and 32 cells (training parameters: 178 849) RMSprop optimizer with learning rate 0.001 | 0.9918 ± 0.0063 | 0.9830 ± 0.0049 | 0.9860 ± 0.0076 | 0.9913 ± 0.0098 |

Note: For each model, the average and standard deviation of five runs are presented.

In the context of the investigation, islanding condition is categorized as the positive class (Class 1), while the non-islanding case serves as the negative class (Class 0). This binary classification setup allows to analyze two distinct types of errors that each classifier might make. The first error type corresponds to a false positive (FP), signifying a false indication of islanding. Conversely, the second error type represents a false negative (FN), denoting a failure to detect an actual islanding event. Assessing the effectiveness of any classifier hinges upon minimizing these two error types. Commonly, the optimization objective is achieved by maximizing accuracy, defined as:

$$A_{\text{Accuracy}} = \frac{T_{\text{P}} + T_{\text{N}}}{T_{\text{P}} + T_{\text{N}} + F_{\text{P}} + F_{\text{N}}} \tag{7}$$

where $T_{\text{P}}$ and $T_{\text{N}}$ signifies true positives and negatives, respectively; $F_{\text{P}}$ and $F_{\text{N}}$ denotes false positives and negatives, respectively. However, in scenarios characterized by unbalanced datasets (e.g., in our case where the test dataset includes 448 islanding and 168 non-islanding), accuracy can be misleading. The reason lies in the potential for a no-skill model, which arbitrarily assigns the majority class to all instances, to exhibit high accuracy. To address this issue and provide a more comprehensive evaluation, alternative metrics are used [50]:

$$
\begin{aligned}
B_{\text{Balanced Accuracy}} &= \frac{1}{2}\left(\frac{T_{\text{P}}}{T_{\text{P}}+F_{\text{N}}}+\frac{T_{\text{N}}}{T_{\text{N}}+F_{\text{P}}}\right)\\
P_{\text{Precision}} &= \frac{T_{\text{P}}}{T_{\text{P}}+F_{\text{P}}}\\
R_{\text{Recall}} &= \frac{T_{\text{P}}}{T_{\text{P}}+F_{\text{N}}}\\
S_{\text{F1-score}} &= 2\times\frac{P_{\text{Precision}}\times R_{\text{Recall}}}{P_{\text{Precision}}+R_{\text{Recall}}}
\end{aligned}
\tag{8}
$$

To rigorously evaluate the performance of the proposed models in the study, the metrics outlined in (7) are employed. These metrics provide a much clearer understanding of the classifiers' capabilities in the presence of unbalanced datasets.

### *B. WaveNet Islanding Detection*

In assessing the effectiveness of the WaveNet classifier model, the primary focus is to prevent overfitting. To achieve this, the model's performance is closely monitored using a validation dataset. Figure 7 visually illustrates the evolution of the training and validation loss functions across training epochs. An early stopping is incorporated during training with a patience parameter set to 10 to ensure that the model's learning process is terminated when no improvement is seen over a specified number of epochs (10 in this case), thereby effectively mitigating the risk of overfitting. Analysis of Fig. 7 reveals that the WaveNet model shows resilience against overfitting. The loss functions converge to stable values after a certain number of training epochs, highlighting the model's ability to generalize effectively.

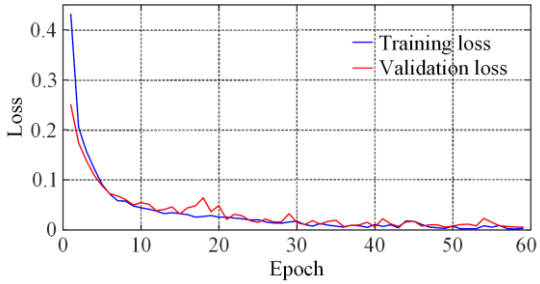


Fig. 7. An exemplar representation showcasing the loss of the model during the training of the WaveNet classifier.

The comprehensive outcomes of all models, as evaluated by the presented metrics, are summarized in Table II. The models based on the methods described in [27] and [28] are rigorously fine-tuned with the dataset to optimize their performance for islanding detection. This tuning ensured that each model is evaluated in optimal conditions specific to the data distribution, providing a fair comparison. The results in Table II are reported as the mean and standard deviations of the performance metrics across five independent runs. A key finding in this analysis is the superior performance of the proposed WaveNet-based classifier, which achieves high accuracy with notably reduced model complexity. Specifically, the WaveNet model uses 89 505 parameters, compared to the 178 849 parameters required by the LSTM-based classifier. Despite its more compact architecture, the WaveNet classifier demonstrates a higher balanced accuracy, achieving an average of 99.81%, outperforming other state-of-the-art methods. This efficiency in learning, coupled with high accuracy, highlights the potential of WaveNet-based models in real-time detection applications, where model simplicity and computational efficiency are of importance. Furthermore, the WaveNet classifier shows a significantly lower standard deviation across performance metrics than the LSTM classifier. This indicates that the WaveNet model generalizes better to new data and is less susceptible to performance fluctuations across different runs and in noisy environments.

Figure 8 provides a visual comparison of the performance of the WaveNet and LSTM classifiers through receiver operating characteristics (ROC) and Precision-Recall curves. Figure 8(a) shows that the WaveNet classifier has a higher precision across a range of recall values compared to the LSTM classifier, indicating that the WaveNet model consistently maintains a low false positive rate even as it correctly identifies a greater number of true islanding events. This behavior is critical in scenarios where false positives (incorrectly signaling islanding) can lead to unnecessary corrective actions, disrupting operations and incurring additional costs. Moreover, the WaveNet classifier's Precision-Recall curve shows a higher AUC, revealing its ability to maintain high recall without significantly compromising precision. In Fig. 8(b), it can also be seen that the WaveNet classifier not only has a higher AUC but also has a higher TPR for small FPR values. This is important in islanding detection applications, where false alarms (high FPR) can lead to costly and unnecessary interventions, while missed detections (low TPR) can result in critical safety risks.

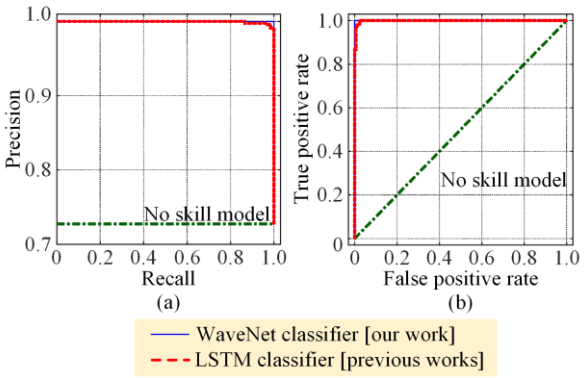


Fig. 8. A comparison between the proposed WaveNet classifier and LSTM classifier inspired by [27], [28], conducted on test data samples, focusing on two curves. (a) The precision-recall curve. (b) The receiver operating characteristic curve.

To establish a baseline, we are considering the no-skill model, which is a dummy classifier that randomly assigns class labels without considering the input. As a result, the no-skill model has a true positive rate that is equal to its false positive rate. Its precision-recall curve appears as a horizontal line, representing the proportion of positive (islanding) samples compared to the total.

### *C. Islanding Detection with Features Denoising UNet*

In this section, the robustness of the proposed models is investigated empirically against noisy features. To this end, the WaveNet and LSTM classifiers are tested with noisy features to determine islanding cases. Table III lists the performance of these models at different noise levels based on balanced accuracy. As expected, noisy features, especially after SNR 15 dB, extensively degrade the models' performance although the WaveNet classifier is more robust to noisy features than the LSTM classifier.

Based on this, the WaveNet islanding detector is equipped with a pre-trained UNet denoising mechanism that dynamically acts as an adaptor during inference, performing real-time denoising without requiring prior knowledge of the noise severity. In this work, a UNet model consisting of an encoder-decoder framework with skip connections to preserve spatial information during down-sampling and up-sampling operations is used. In the encoder part, two consecutive 1D convolutional layers with 32 filters each and ReLU activation function are employed, followed by max-pooling with a pool size of 2 to down-sample the input signals effectively. After that, two additional convolutional layers each with 64 filters and ReLU activation are applied, followed by a max-pooling layer. This stage further abstracts features and serves as the bottleneck of the network. The decoder confidently up-samples the feature maps to the original input resolution. It starts with up-sampling followed by concatenation with feature maps from the corresponding encoder stage. Then, two convolutional layers with 64 filters each and ReLU activation are applied. Another up-sampling operation is performed, followed by concatenation and two more convolutional layers with 32 filters each and ReLU activation. Finally, a 1D convolutional layer with 6 filters (number of features) generates the denoised output signals. In this work, the UNet model is pre-trained at SNR 15 dB and is used for all noise levels where the Adam optimizer with a learning rate of 0.0002 optimizes the UNet parameters by minimizing the mean absolute error (MAE) loss function.

In Fig. 9, it is clear that the UNet model can minimize the MAE loss function without overfitting. In addition, the results of islanding detection with UNet feature denoising at different levels of noise are presented in Table III. The table shows that the LSTM-based classifier exhibits a significant decline in accuracy as noise level increases. For example, at 10 dB SNR, the LSTM classifier's accuracy drops to 93.77%, indicating its sensitivity to moderate noise interference. In contrast, the WaveNet+UNet classifier maintains an accuracy of 98.31% at the same noise level, demonstrating that the integrated denoising UNet component effectively mitigates moderate noise and preserves critical features for accurate islanding detection. In more severe noise conditions, such as at 5 dB, the disparity between the two models becomes even more pronounced. The LSTM model's accuracy declines further to 90.08%, a significant drop that indicates the model's limited capacity to filter out extensive noise. Conversely, the WaveNet+UNet model achieves an accuracy of 95.4% under the same conditions, outperforming the LSTM-based model by over 5%. Additionally, the smaller standard deviation in the WaveNet+UNet model, especially in high-noise settings, emphasizes the robustness and adaptability of its denoising mechanism. This robust performance underscores the efficacy of the UNet's denoising capability in preserving key features despite high noise interference, enabling the WaveNet classifier to make more accurate predictions.

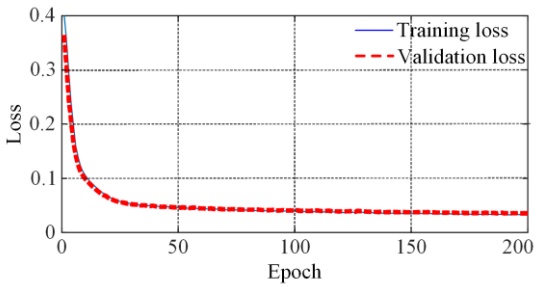


Note: The tiny gap between the training and validation losses ensures that the model is not overfitting.

Fig. 9. The loss function of UNet denoising model versus training epochs.

TABLE III
COMPARING MODELS BASED ON BALANCED ACCURACY IN THE PRESENCE OF NOISE

| Model | 20 dB | 15 dB | 10 dB | 5 dB |
|---|---|---|---|---|
| LSTM classifier (state-of-the-art [27], [28]) | 0.9698 ± 0.0044 | 0.9612 ± 0.0081 | 0.9306 ± 0.0204 | 0.8912 ± 0.0125 |
| WaveNet classifier (proposed) | 0.9889 ± 0.0023 | 0.9731 ± 0.0077 | 0.9390 ± 0.0090 | 0.9166 ± 0.0099 |
| WaveNet classifier with denoising UNet (proposed) | 0.9925 ± 0.0019 | 0.9907 ± 0.0069 | 0.9831 ± 0.0073 | 0.9538 ± 0.0090 |

Note: Average and one standard deviation of five runs are displayed for each model.

### *D. NDZ Analysis*

A key criterion for islanding detection methods is the non-detection zone (NDZ). In this area, the power imbalance at the point of common coupling (PCC) is evaluated when the islanding detection method is unable to identify islanding in most cases. Typically, this occurs within the zero active/reactive power mismatch range. The values of $\Delta P$ and $\Delta Q$ are determined as:

$$\begin{aligned} \Delta P &= P_{\text{Load}} - P_{\text{DG}} \\ \Delta Q &= Q_{\text{Load}} - Q_{\text{DG}} \end{aligned} \tag{9}$$

where $P_{\text{Load}}$ and $Q_{\text{Load}}$ represent the active and reactive power demands of the load; while $P_{\text{DG}}$ and $Q_{\text{DG}}$ denote the active and reactive power supplied by the resources. To examine the critical range of the NDZ, 605 separate islanding operating test points are conducted within ±0.008 p.u. for $\Delta P$ and ±0.03 p.u. for $\Delta Q$, performed with a precision of 0.001 p.u. for $\Delta P$ and 0.002 p.u. for $\Delta Q$ (zero and near-zero power mismatch). In Fig. 10, the yellow area represents the zone where the NDZ test has been conducted, while the blue dots represent events in which the proposed method accurately identifies islanding conditions. Only five islanding events, marked in red, remain undetected. In this test, all ranges with the specified accuracy have been evaluated, and all points with $\Delta P = 0$ and $\Delta Q = 0$ have also been included in this evaluation. This encompasses all aspects in contrast to [33], which exhibits a NDZ of 0.0125 p.u., and [51], which presents a range of 0.09 p.u. Therefore, it can be concluded that the proposed method has near zero NDZ and can successfully detect islanding events in almost any power mismatch condition.

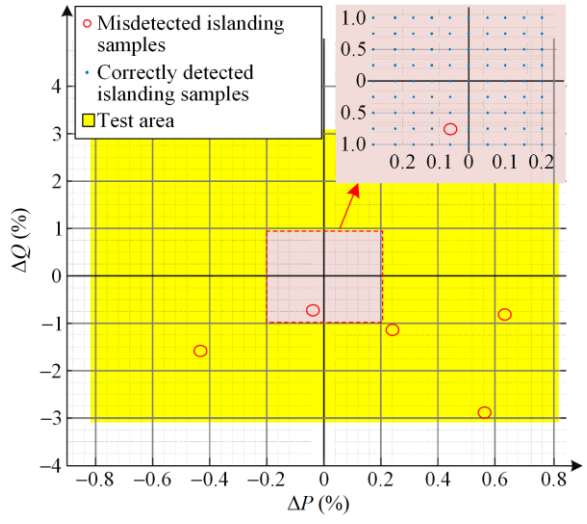


Fig. 10. NDZ analyses with 605 separate islanding operating test points (zero and near-zero power mismatch)

## V. Conclusion

In this paper, an innovative WaveNet classifier equipped with a pre-trained denoising UNet is introduced for islanding detection in active distribution networks. Unlike other state-of-the-art models, such as LSTM, which may face challenges such as gradient vanishing and instability, the WaveNet classifier employs a straightforward 1D convolutional architecture with skip connections to enhance prediction accuracy while ensuring stability. This approach uses fewer parameter than LSTM, thereby improving the efficiency and simplicity of the detection system while reducing implementation costs. To address the challenges associated with islanding detection in noisy conditions, a UNet model including an encoder-decoder framework and skip connections is used. This strategy ensures the robustness of the detection algorithm against significant system noise, achieving an accuracy of 98.31% even under a 10 dB SNR. The validation process involves comprehensive testing across various real-world scenarios, representing both islanding and non-islanding conditions. These scenarios include different load active/reactive power values, load switching transients, capacitor bank switching, fault conditions in the main grid, diverse load quality factors, and varying SNR levels. The use of a realistic test system and the integration of both conventional and inverter-based resources further strengthen the credibility of the analysis. Overall, the proposed model showcases a substantial improvement in islanding detection accuracy, particularly in noisy environments. Finally, a comparative analysis with the state-of-the-art LSTM classifier highlights the superiority of the proposed approach in terms of lower model complexity, e.g., with 89 505 learning parameters for WaveNet compared to 178 849 for LSTM, as well as greater stability and generalization, evidenced by a significantly lower standard deviation of evaluation metrics.

## Acknowledgment

Not applicable.

## Authors' Contributions

Amirhosein Alizadeh: conceptualization, data curation, formal analysis, investigation, methodology, resources, software, validation, visualization, writing-original draft, and writing-review & editing. Seyed Fariborz Zarei: conceptualization, formal analysis, methodology, project administration, resources, supervision, validation, writing-original draft, and writing-review & editing. Mohammadhadi Shateri: conceptualization, data curation, formal analysis, investigation, methodology, project administration, resources, software, supervision, validation, visualization, writing-original draft, and writing-review & editing. All authors read and approved the final manuscript.

## FUNDING

This work is carried out without the support of any funding agency.

## AVAILABILITY OF DATA AND MATERIALS

Not applicable.

## DECLARATIONS

Competing interests: The authors declare that they have no known competing financial interests or personal relationships that could have appeared to influence the work reported in this article.

## AUTHORS' INFORMATION

**Amirhosein Alizadeh** holds a B.Sc. in electrical engineering (2012) and is currently pursuing an M.Sc. in electrical power engineering at Qom University of Technology, Qom, Iran. His research focuses on power grid protection, anti-islanding protection, and active distribution networks. Professionally, he has extensive experience in industrial design, monitoring systems, control and protection of electric energy systems, and the design of industrial power networks and grid-connected generators since 2014.

**Seyed Fariborz Zarei** received his B.Sc. degree in electrical engineering from the Department of Electrical Engineering at Amirkabir University of Technology (Tehran Polytechnic), Tehran, Iran, in 2012. He continued his academic pursuits by achieving both his M.Sc. and Ph.D. degrees in electrical engineering from the Department of Electrical Engineering at Sharif University of Technology, Tehran, Iran, in 2014 and 2019, respectively. From February to August 2018, he served as a visiting Ph.D. scholar at the Department of Energy, Aalborg University, Aalborg, Denmark. In January 2021, Dr. Zarei joined Qom University of Technology, Qom, Iran, as an assistant professor in the Department of Electrical and Computer Engineering, Dr. Zarei has authored over 40 conference and journal papers in the field of power electronics and electrical power engineering. His research is centered on the application of power electronics systems in power grids, with a focus on modeling, control, protection, and stability aspects. Additionally, Dr. Zarei established the Power-Electronic and Grid Laboratory at Qom University of Technology in January 2022. This laboratory conducts studies on DC/AC converters and their interaction with the AC power grid. The experimental platform of the laboratory offers a flexible environment for implementing diverse control methodologies on three-phase converters, facilitating investigations into control, protection, and stability aspects.

**Mohammadhadi Shateri** received the B.Sc. degree in electrical engineering from the Amirkabir University of Technology, Tehran, Iran, in 2012, the M.Sc. degree in electrical engineering from the University of Manitoba, Winnipeg, Canada, in 2017, and the Ph.D. in electrical engineering from McGill University, Montreal, Canada, in 2021. He is currently an assistant professor with École de technologie supérieure, Université du Québec in Montreal, Canada. He is also a member of LIVIA-Laboratoire d'imagerie, de vision et d'intelligence artificielle-at ÉTS university. His research interests include machine learning, deep generative modeling, security of learning systems and the secure processing of information with applications to computer vision and health among others.

## REFERENCES

[1] B. Chaitanya, A. Yadav, and M. Pazoki *et al.*, "A comprehensive review of islanding detection methods," *Uncertainties in Modern Power Systems*, pp. 211-256, Nov. 2021.

[2] S. Dutta, P. K. Sadhu, and M. J. B. Reddy *et al.*, "Shifting of research trends in islanding detection method-a comprehensive survey," *Protection and Control of Modern Power Systems*, vol. 3, no. 1, pp. 1-20, Jan. 2018.

[3] F. Mumtaz, K. Imran, and A. Abusorrah *et al.*, "An extensive overview of islanding detection strategies of active distributed generations in sustainable microgrids," *Sustainability,* vol. 15, no. 5, Mar. 2023.

[4] L. Chen, X. Dong, and B. Wang *et al.*, "An edge computing-oriented islanding detection using differential entropy and multi-support vector machines," *IEEE Transactions on Smart Grid*, vol. 15, no. 1, pp. 191-202, Jun. 2023.

[5] O. Dharmapandit, R. Patnaik, and P. Dash, "A fast time-frequency response based differential spectral energy protection of AC microgrids including fault location," *Protection and Control of Modern Power Systems*, vol. 2, no. 4, pp. 1-28, Oct. 2017.

[6] O. Arguence, F. Cadoux, and B. Raison *et al.*, "Impact of power regulations on unwanted islanding detection," *IEEE Transactions on Power Electronics*, vol. 33, no. 10, pp. 8972-8981, Dec. 2017.

[7] IEEE standard for interconnection and interoperability of distributed energy resources with associated electric power systems interfaces, I. S. 1547-2018, Apr. 2018.

[8] C. R. Reddy, B. S. Goud, and B. N. Reddy *et al.*, "Review of islanding detection parameters in smart grids," in *2020 8th International Conference on Smart Grid (icSmartGrid)*, Paris, France, Jun. 2020, pp. 78-89.

[9] R. Bakhshi-Jafarabadi, J. Sadeh, and A. Serrano-Fontova *et al.*, "Review on islanding detection methods for grid-connected photovoltaic systems, existing limitations and future insights," *IET Renewable Power Generation*, vol. 16, no. 15, pp. 3406-3421, Jul. 2022.

[10] M. Grebla, J. R. Yellajosula, and H. K. Høidalen, "Adaptive frequency estimation method for ROCOF islanding detection relay," *IEEE Transactions on Power Delivery*, vol. 35, no. 4, pp. 1867-1875, Nov. 2019.

[11] R. Chandrakar, R. K. Dubey, and B. K. Panigrahi, "THD-based passive islanding detection technique for droop-controlled grid-forming inverters," *IEEE Systems Journal,* vol. 17, no. 4, pp. 5750-5761, Jun. 2023.

[12] J. Xing and L. Mu, "A novel islanding detection method for distributed PV system based on μPMUs," *IEEE Transactions on Smart Grid*, vol. 14, no. 5, pp. 3696-3706, Jan. 2023.

[13] R. Bakhshi-Jafarabadi, J. Sadeh, and M. Popov, "Maximum power point tracking injection method for islanding detection of grid-connected photovoltaic systems in microgrid," *IEEE Transactions on Power Delivery*, vol. 36, no. 1, pp. 168-179, Feb. 2020.

[14] R. L. Lima, J. P. Bonaldo, and J. C. Vieira *et al.*, "A graphical method to assess the technical feasibility of intentional islanding of distributed synchronous generators," *IEEE Transactions on Power Delivery*, vol. 38, no. 1, pp. 742-745, Nov. 2022.

[15] Y. Bansal and R. Sodhi, "A statistical features based generic passive islanding detection scheme for IIDGs system," *IEEE Transactions on Power Delivery*, vol. 37, no. 4, pp. 3176-3188, Nov. 2021.

[16] M. R. Alam, M. T. A. Begum, and B. Mather, "Islanding detection of distributed generation using electrical variables in space vector domain," *IEEE Transactions on Power Delivery*, vol. 35, no. 2, pp. 861-870, Jul. 2019.

[17] R. Bekhradian and M. Sanaye-Pasand, "A comprehensive survey on islanding detection methods of synchronous generator-based microgrids: issues, solutions and future works," *IEEE Access*, vol. 10, pp. 76202-76219, Jul. 2022.

[18] N. Gupta, R. Dogra, and R. Garg *et al.*, "Review of islanding detection schemes for utility interactive solar photovoltaic systems," *International Journal of Green Energy*, vol. 19, no. 3, pp. 242-253, Jun. 2022.

[19] E. Kazeminia, S. Goudarzitaemeh, and S. Eren *et al.*, "Modeling and stability analysis of an active islanding detection method in DC microgrids using real-time wavelet analysis," *IEEE Access*, vol. 12, pp. 53767-53784, Apr. 2024.

[20] S. S. Mohapatra, M. K. Maharana, and S. B. Pati, "Comprehensive review to analyze the islanding in distributed generation system," in *2021 1st International Conference on Power Electronics and Energy (ICPEE)*, Bhubaneswar, India, Jan. 2021, pp. 1-7.

[21] A. Hussain, C.-H. Kim, and A. Mehdi, "A comprehensive review of intelligent islanding schemes and feature selection techniques for distributed generation system," *IEEE Access*, vol. 9, pp. 146603-146624, Oct. 2021.

[22] M. Karimi, M. Farshad, and R. Azizipanah-Abarghooee *et al.*, "Harmonic signature-based one-class classifier for islanding detection in microgrids," *IEEE Systems Journal*, vol. 17, no. 4, pp. 5889-5898, Jun. 2023.

[23] M.-S. Kim, R. Haider, and G.-J. Cho *et al.*, "Comprehensive review of islanding detection methods for distributed generation systems," *Energies*, vol. 12, no. 5, Mar. 2019.

[24] B. Matic-Cuka and M. Kezunovic, "Islanding detection for inverter-based distributed generation using support vector machine method," *IEEE Transactions on Smart Grid*, vol. 5, no. 6, pp. 2676-2686, Aug. 2014.

[25] S. Vyas, R. Kumar, and R. Kavasseri, "Multivariate statistics and supervised learning for predictive detection of unintentional islanding in grid-tied solar PV systems," *Applied Computational Intelligence and Soft Computing*, vol. 2016, no. 1, Mar. 2016.

[26] M. Massaoudi, H. Abu-Rub, and S. S. Refaat *et al.*, "Deep learning in smart grid technology: a review of recent advancements and future prospects," *IEEE Access*, vol. 9, pp. 54558-54578, Apr. 2021.

[27] Y. Xia, F. Yu, and X. Xiong *et al.*, "A novel microgrid islanding detection algorithm based on a multi-feature improved LSTM," *Energies*, vol. 15, no. 8, Apr. 2022.

[28] A. A. Abdelsalam, A. A. Salem, and E. S. Oda *et al.*, "Islanding detection of microgrid incorporating inverter based DGs using long short-term memory network," *IEEE Access*, vol. 8, pp. 106471-106486, Jun. 2020.

[29] A. K. Özcanlı and M. Baysal, "A novel multi-LSTM based deep learning method for islanding detection in the microgrid," *Electric Power Systems Research*, vol. 202, Sep. 2022.

[30] A. Yılmaz and G. Bayrak, "A new signal processing-based islanding detection method using pyramidal algorithm with undecimated wavelet transform for distributed generators of hydrogen energy," *International Journal of Hydrogen Energy*, vol. 47, no. 5, pp. 19821-19836, May 2022.

[31] S. B. A. Bukhari, K. K. Mehmood, and A. Wadood *et al.*, "Intelligent islanding detection of microgrids using long short-term memory networks," *Energies*, vol. 14, no. 18, Sep. 2021.

[32] J. A. Pinto, K. P. Vittal, and K. M. Sharma, "Passive islanding detection scheme based on instantaneous voltage & current for a multi-DG microgrid," *IEEE Access*, vol. 12, pp. 160715-160727, Oct. 2024.

[33] S. T. Chauhdary, M. H. Baloch, and M. Alqahtani *et al.*, "Fast passive anti-islanding strategy for AC microgrids using cubature Kalman filtering algorithm," *IEEE Access*, vol. 12, pp. 85608-85621, Jun. 2024.

[34] S. T. Chauhdary, F. Mumtaz, and H. A. Sher *et al.*, "Particle filter-based passive islanding detection scheme for renewable energy penetrated distribution systems," *IEEE Access*, vol. 12, pp. 147501-147515, Oct. 2024.

[35] N. K. Swarnkar, O. P. Mahela, and B. Khan *et al.*, "Identification of islanding events in utility grid with renewable energy penetration using current based passive method," *IEEE Access*, vol. 9, pp. 93781-93794, Jun. 2021.

[36] S. Chandak, M. Mishra, and S. Nayak *et al.*, "Optimal feature selection for islanding detection in distributed generation," *IET Smart Grid*, vol. 1, no. 3, pp. 85-95, Sep. 2018.

[37] A. Hussain, C. H. Kim, and S. Admasie, "An intelligent islanding detection of distribution networks with synchronous machine DG using ensemble learning and canonical methods," *IET Generation, Transmission & Distribution*, vol. 15, no. 23, pp. 3242-3255, Jul. 2021.

[38] B. K. Chaitanya, A. Yadav, and M. Pazoki, "An advanced signal decomposition technique for islanding detection in DG system," *IEEE Systems Journal*, vol. 15, no. 3, pp. 3220-3229, Aug. 2020.

[39] A. Hussain, C.-H. Kim, and M. S. Jabbar, "An intelligent deep convolutional neural networks-based islanding detection for multi-DG systems," *IEEE Access*, vol. 10, pp. 131920-131931, Dec. 2022.

[40] A. Van Den Oord, S. Dieleman, and H. Zen *et al.*, "Wavenet: a generative model for raw audio," in *The 9th ISCA Speech Synthesis Workshop*, Sep., 2016.

[41] J. C. Quispe and E. Orduña, "Transmission line protection challenges influenced by inverter-based resources: a review," *Protection and Control of Modern Power Systems*, vol. 7, no. 3, pp. 1-17, Jul. 2022.

[42] F. Erdiwansyah, F. Mahidin, and H. Husin *et al.*, "A critical review of the integration of renewable energy sources with various technologies," *Protection and Control of Modern Power Systems*, vol. 6, pp. 1-18, Feb. 2021.

[43] P. Dhal and C. Azad, "A comprehensive survey on feature selection in the various fields of machine learning," *Applied Intelligence*, vol. 52, no. 4, pp. 4543-4581, Jul. 2022.

[44] T. M. C. A. J. A. Thomas, "Elements of information theory," *2nd edition*. Willey-Interscience: NJ, 2006.

[45] Y. Bengio, P. Simard, and P. Frasconi, "Learning long-term dependencies with gradient descent is difficult," *IEEE Transactions on Neural Networks*, vol. 5, no. 2, pp. 157-166, Mar. 1994.

[46] S. Hochreiter and J. Schmidhuber, "Long short-term memory," *Neural Computation*, vol. 9, no. 8, pp. 1735-1780, Nov. 1997.

[47] F. A. Gers, J. Schmidhuber, and F. Cummins, "Learning to forget: continual prediction with LSTM," *Neural Computation*, vol. 12, no. 10, pp. 2451-2471, Aug. 2000.

[48] K. He, X. Zhang, and S. Ren *et al.*, "Deep residual learning for image recognition," in *Proceedings of the IEEE Conference on Computer Vision and Pattern Recognition*, pp. 770-778, Dec. 2016.

[49] O. Ronneberger, P. Fischer, and T. Brox, "UNet: convolutional networks for biomedical image segmentation," in *18th International Conference proceedings on Medical Image Computing and Computer-Assisted Intervention–MICCAI 2015*, Munich, Germany, Oct. 2015, pp. 234-241.

[50] T. Saito and M. Rehmsmeier, "The precision-recall plot is more informative than the ROC plot when evaluating binary classifiers on imbalanced datasets," *PloS One*, vol. 10, no. 3, Mar. 2015.

[51] S. Raza, H. M. Munir, and N. Shafique *et al.*, "Implementation of islanding recognizing technique for wind distributed generations considering insignificant NDZ," *Frontiers in Energy Research*, vol. 10, Jan. 2022.